Earthquakes and Structures, *Vol. 29, No. 4 (2025) 311-329*
https://doi.org/10.12989/eas.2025.29.4.311

Experimental investigation on in-plane structural performance of half-PC slab-wall joints with various reinforcing details

Jae Hyun Kim[1a], Sun-Jin Han[2b], Cha-Young Yun[1c], Hoseong Jeong[1a], Min-Kook Park[1a] and Kang Su Kim*[3]

[1]Department of Architectural Engineering, University of Seoul, 163 Siripdae-ro, Dongdaemun-gu, Seoul 02504, Korea
[2]Department of Architectural Engineering, Jeonju University, 303 Cheonjam-ro, Wansan-gu, Jeonju-si, Jeonbuk-do 55069, Korea
[3]Department of Architectural Engineering and the Smart City Interdisciplinary Major Program, University of Seoul, 163 Siripdae-ro, Dongdaemun-gu, Seoul 02504, Korea

(Received June 16, 2025, Revised August 25, 2025, Accepted August 26, 2025)

Abstract. In this study, quasi-static cyclic loading tests were conducted to evaluate the in-plane structural performance of half-precast concrete slab-wall joints. Nine full-scale specimens were fabricated, with key test variables that include the system type, anchorage type, number of anchorage reinforcements, and slab type. The structural performance was assessed in terms of the lateral load-displacement behavior, maximum load capacity, stiffness retention ability, and energy dissipation capacity. The results showed that the monolithic reinforced concrete specimens exhibited superior performance compared to the half-precast concrete specimens. However, the half-precast concrete specimens exceeded the nominal shear strength requirements specified in ACI 318-19. Among the half-precast concrete specimens, the anchorage type and slab type had negligible effects on the overall performance, whereas an increase in the number of anchorage reinforcements unexpectedly resulted in degraded performance. Analysis of the local shear strength of the anchorage reinforcements revealed that those in the half-precast concrete specimens failed to achieve the intended shear capacity, primarily because of insufficient development length. Based on these findings, a modified nominal shear strength model incorporating the anchorage development length was proposed.

Keywords: cyclic loading test; in-plane structural behavior; precast concrete; reinforced concrete; slab-wall joint; structural performance

1. Introduction

Recently, the construction industry has shown growing interest in precast concrete (PC) systems, which involve the systematic, factory-based production of structural members. This shift from conventional reinforced concrete (RC) systems has been mainly driven by the increasing costs of labor and materials (Kurama *et al.* 2018). In PC systems, structural members are fabricated in a factory, transported to a construction site, and assembled on-site, thereby minimizing on-site work and enhancing the overall quality of the structural members. Depending on the fabrication and assembly methods of the precast members, PC systems can be categorized into full- and half-PC systems. A full-PC system is a dry construction method in which all the structural members are prefabricated and subsequently assembled on-site. This system offers advantages such as rapid construction, improved quality control, and reduced on-site labor, each of which is maximized. However, it also entails high initial manufacturing costs, the need for large-scale equipment during transportation and erection, and technical challenges in ensuring structural integrity between members owing to difficulties in joint design and construction (Arditi *et al.* 2000). By contrast, a half-PC system is a hybrid construction method in which factory-fabricated PC members are placed on-site and integrated with cast-in-place concrete to complete the structure. This process has the advantage of ensuring both structural integrity and economic efficiency with the precision of factory manufacturing and flexibility of on-site construction (Lee *et al.* 2016). Nonetheless, the effective implementation of the half-PC system requires further empirical verification of its structural performance with respect to joint detailing and substantial effort to ensure its applicability across diverse construction environments.

Half-PC systems have been widely adopted in industrial buildings and modular housing, where construction follows a systematic and repetitive process (Kim *et al.* 2023). These systems have also been applied to residential buildings in the form of wall systems, which allow for a reduced story height compared to moment-resisting frame systems, offering both economic and construction-related advantages. However, similar to other PC systems, the structural integrity of the half-PC wall system must be rigorously verified with respect to joint detailing, and serviceability issues such as excessive cracking and water leakage must also be evaluated (Zhang *et al.* 2020, Kim *et al.* 2021).

As shown in Fig. 1, joints in wall systems are subjected

*Corresponding author, Professor
E-mail: kangkim@uos.ac.kr
[a]Ph.D.
[b]Professor
[c]M.S.

ISSN: 2092-7614 (Print), 2092-7622 (Online)

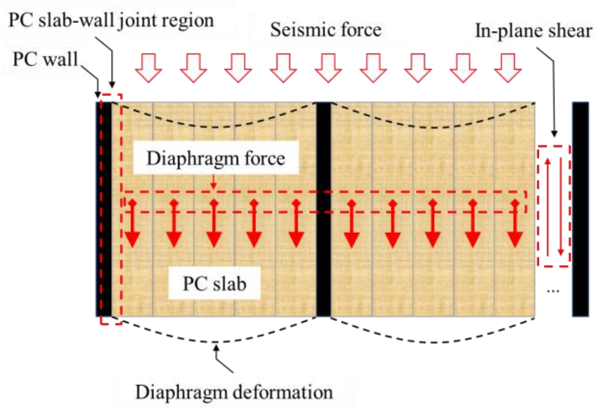

Fig. 1 In-plane diaphragm action and force transfer in a PC wall system

to both out-of-plane behavior due to gravity loads and in-plane behavior (i.e., diaphragm action) due to seismic loads (Fleishman *et al.* 2005, Fleishman *et al.* 2013). Unlike out-of-plane behavior, the in-plane behavior involves significant shear forces under lateral loading, and its characteristics are highly sensitive to the joint reinforcement details. Therefore, many studies have focused on evaluating the in-plane behavior of PC wall systems (Zhang *et al.* 2011, 2019, Zhang and Fleischman 2016, Ren and Naito 2013, Brunesi *et al.* 2018, Pang *et al.* 2020, Zhou *et al.* 2021). Fleischman *et al.* (2005, 2013) conducted extensive experimental and analytical studies on the behavior of slab-slab joints to ensure adequate diaphragm behavior in prestressed PC floor systems located in high-seismicity regions. Zhang *et al.* (2011, 2019) and Zhang and Fleischman (2016) examined the key parameters affecting diaphragm response and proposed an improved seismic design methodology for prestressed PC floor systems. Ren and Naito (2013) evaluated various PC slab-slab joint details through comparative testing to identify appropriate configurations for different performance levels. Brunesi *et al.* (2018) performed cyclic tests on full-scale two-story PC specimens comprising PC slabs and walls connected by dowel bars and steel angles to assess their structural performance. Pang *et al.* (2020) developed a new PC slab-slab joint system incorporating hairpin connectors and cover plates, and validated its structural performance through experiments, subsequently proposing an equivalent beam model. Zhou *et al.* (2021) conducted experimental and analytical studies on the PC wall system using box connectors and post-tensioning. In addition, various studies have been conducted to evaluate and enhance the structural and seismic performance of joints in PC wall systems (Zheng and Oliva 2005, Lim *et al.* 2016, Tsampras *et al.* 2017, Zhi *et al.* 2017, Yun *et al.* 2025).

Nevertheless, most previous studies have primarily focused on slab-slab joints in full-PC or half-PC systems, which limits the experimental data available for slab-wall joint. This research trend is assumed to be because PC slab-slab joints occur repeatedly in almost all PC systems, making them a more common focus of investigation. By contrast, PC slab-wall joints are primarily found in the PC wall system, and their structural role has often been implicitly assumed based on the findings from PC slab-slab joint studies rather than being directly investigated. Moreover, PC slab-wall joints involve greater challenges in fabricating test specimens and conducting experiments under realistic boundary conditions. Therefore, in this study, full-scale test specimens were fabricated based on the joint details of a five-story modular house in South Korea, and quasi-static cyclic loading tests were performed to investigate the in-plane structural performance of slab-wall joints in half-PC systems.

2. Experimental program

2.1 Details of test specimens

Nine slab-wall joint specimens were fabricated in this study, with the system type, anchorage type, number of anchorage reinforcements, and slab type as key variables. The details of the test specimens are summarized in Table 1. As shown in Fig. 2, 90° standard hook, headed bar, U-shaped bar and combined types were considered as anchorage types. Notably, the slab-wall joint is a highly congested region where the longitudinal, auxiliary, and anchorage reinforcements intersect. Owing to the complexity of reinforcement detailing, ensuring both constructability and sufficient anchorage performance is challenging. To address this issue, a U-shaped bar detail was introduced as a test variable. In this detail, two auxiliary U-shaped bars were connected orthogonally to the end of a single straight bar, allowing for easier field installation (refer to Fig. 2(c)). The auxiliary bars and the straight bar were tied together using tie wires, which are widely employed in practice as the common method of bar fastening, thereby enhancing the constructability of the U-shaped bar. Regarding the number of anchorage reinforcements (n_a), three cases were considered based on the slab width (=1,200 mm) of the test specimens: (1) the number of anchorage reinforcements equal to that of the PC prototype (i.e., n_a=4), (2) the number of anchorage reinforcements equal to that of the RC prototype (i.e., n_a=8), and (3) the average of the two (i.e., n_a=6). As previously mentioned, full-scale test specimens were fabricated based on the structural details of an actual five-story modular house, and the slab span length and wall

Table 1 Summary of test specimens

	Specimen Name	RC	Ho0.5T	He0.5T
	System Type	RC	Half-PC	Half-PC
Anchorage Reinforcement	Anchorage Type	90° Standard Hook	90° Standard Hook (Ho)	Headed Bar (He)
	The Number of Reinforcements (n_a)* (Normalized by the Number of Those in the RC Specimen)	8	4 (0.5)	4 (0.5)
	Slab Type	Monolithic Casting	Truss PC Slab (T)	Truss PC Slab (T)
	Specimen Name	U0.5T	U0.75T	U1.0T
	System Type	Half-PC	Half-PC	Half-PC
Anchorage Reinforcement	Anchorage Type	U-Shaped Bar (U)	U-Shaped Bar (U)	U-Shaped Bar (U)
	The Number of Reinforcements (n_a)* (Normalized by the Number of Those in the RC Specimen)	4 (0.5)	6 (0.75)	8 (1.0)
	Slab Type	Truss PC Slab (T)	Truss PC Slab (T)	Truss PC Slab (T)
	Specimen Name	HoU0.5T	HeU0.5T	U0.5H
	System Type	Half-PC	Half-PC	Half-PC
Anchorage Reinforcement	Anchorage Type	90° Standard Hook +U-Shaped Bar (HoU)	Headed Bar +U-Shaped Bar (HeU)	U-Shaped Bar (U)
	The Number of Reinforcements (n_a)* (Normalized by the Number of Those in the RC Specimen)	4 (0.5)	4 (0.5)	4 (0.5)
	Slab Type	Truss PC Slab (T)	Truss PC Slab (T)	Hollow-Core Slab (H)

Nomenclature of Half-PC specimen series

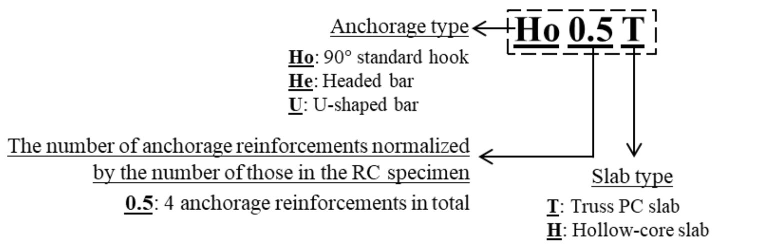

*The number of reinforcements anchored into the slab-wall joint within a slab width of 1,200 mm

(a) 90° standard hook (Ho)

(b) Headed bar (He)

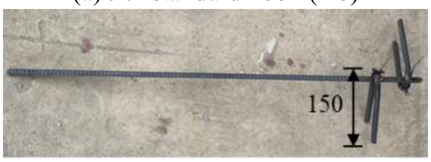

(c) U-shaped bar (U)

(d) 90° standard hook+U-shaped bar (HoU)

(e) Headed bar+U-shaped bar (HeU)

Fig. 2 Various anchorage reinforcement details (unit: mm)

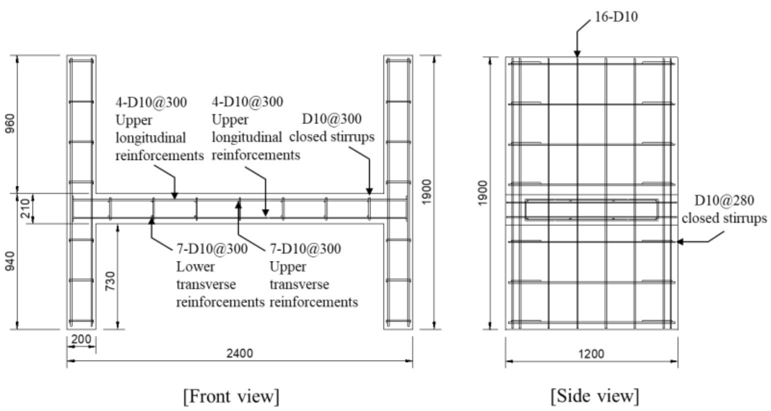

(a) RC specimen

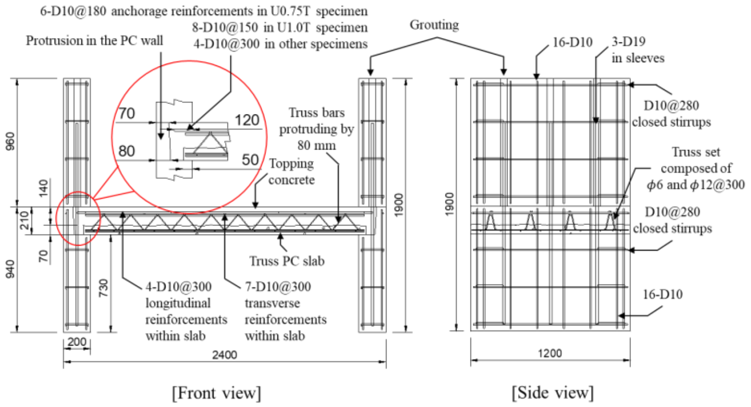

(b) T specimen series

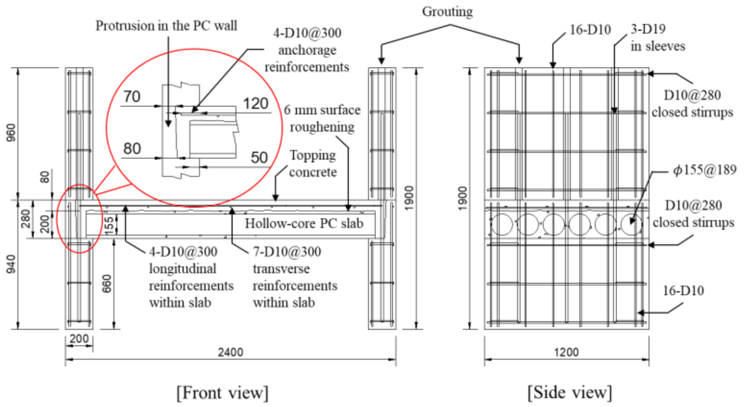

(c) U0.5H specimen

Fig. 3 Dimension details of test specimens (unit: mm)

height were adjusted considering the spatial limitations of the laboratory.

As shown in Fig. 3, the width and length of the slab were 1,200 mm and 2,000 mm (excluding the seating length of the slab), respectively. The slab cross section varied with the slab type. For the specimen with a hollow-core PC slab, the cross-sectional dimensions—including the topping concrete (cast-in-place concrete)—were 1,200 mm×280 mm, whereas for the other specimens, the dimensions were 1,200 mm×210 mm.

In the specimen nomenclature summarized in Table 1, the first letter indicates the anchorage type, as shown in Fig. 2, and the following number represents the ratio of the number of anchorage reinforcements in the specimen to that in the RC specimen. The last letter denotes the slab type. For example, the specimen labeled U0.5T refers to a specimen with four anchorage reinforcements detailed with U-shaped bars and a truss PC slab.

As shown in Fig. 3(a), four D10 longitudinal reinforcements were placed at a spacing of 300 mm along the top and bottom of the RC specimen slab, and seven D10 reinforcements were placed at a spacing of 300 mm as transverse reinforcements. Ten closed stirrups were placed with a spacing of 300 mm. In addition, the D10 longitudinal reinforcements were fully anchored to the wall using 90° standard hooks formed at their ends. The straight extension

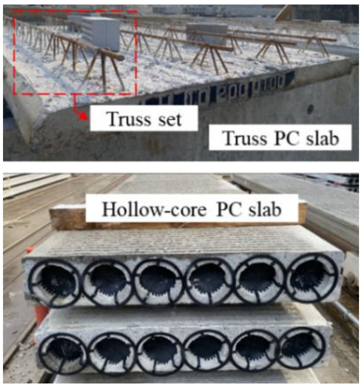

(a) Fabrication of PC slab

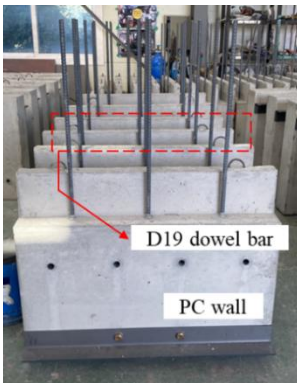

(b) Fabrication of PC wall

(c) Placement of PC slab and installation of top and anchorage reinforcements


(d) Casting of topping concrete

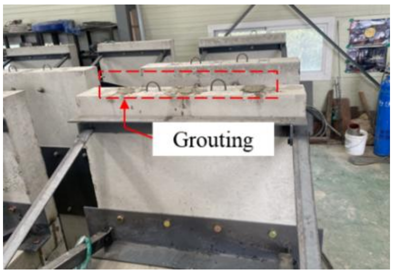

(e) Assembly of upper PC wall and grouting


(f) Monolithic casting of RC specimen

(g) Completion and setup of test specimens

Fig. 4 Fabrication process of test specimens

Table 2 Material properties of the test specimens

Compressive Strength of Concrete/Designed Compressive Strength, $f_c{}'$ [MPa]	Precast Concrete (Wall)		43.0/35.0
	Precast Concrete (Slab)	Truss PC Slab	35.3/35.0
		Hollow-Core PC Slab	58.7/49.0
	Topping Concrete, RC Specimen		20.4/24.0
Compressive Strength of Grout/Designed Compressive Strength [MPa]			45.1/40.0
Yield (tensile) Strength of Reinforcement, $f_y(f_u)$ [MPa]	D10		455.7(568.9)
	D19		516.9(664.1)

of the hook was 150 mm, which satisfied the requirements specified in Table 25.3.1 of ACI 318-19.

As shown in Fig. 3(b), in the T specimen series using a truss PC slab, the slab had a thickness of 70 mm, and truss bars consisting of $\phi6$ and $\phi12$ rebars were placed at a spacing of 300 mm within the cross section. These truss bars extended 80 mm beyond the PC slab to ensure composite action with the topping concrete. In the T specimen series, the topping concrete with a thickness of 140 mm contained four D10 longitudinal reinforcements and seven D10 transverse reinforcements that were spaced identically to the reinforcements in the RC specimen.

Fig. 3(c) shows the details of the U0.5H specimen, which incorporates a hollow-core PC slab with a thickness of 200 mm. Within the slab, circular voids with a diameter of 155 mm were formed with a spacing of 189 mm along the slab width. To ensure full composite action between the hollow-core PC slab and the topping concrete, surface roughening was applied to the upper surface of the slab. The thickness of the topping concrete was 80 mm, and the reinforcement details inside the topping concrete were identical to those in the T specimen series.

The headed bar details used in the He0.5T specimen were fabricated to satisfy the requirements specified in Clause 25.4.4 of ACI 318-19. In addition, for the half-PC specimens, both the 90° standard hooks and U-shaped bars were fabricated with a 150 mm straight extension. In contrast, in the HoU0.5T specimen, which combined the 90° standard hook and U-shaped bar details, the straight extension of the hook was intentionally reduced to 100 mm to evaluate the mutual reinforcement effect between the 90° standard hook and U-shaped bar details. The headed bar details of the HeU0.5T specimen were the same as those of the He0.5T specimen.

The widths and lengths of the walls of the test specimens were 1,200 mm and 1,900 mm, respectively, and the cross-sectional dimensions of the walls were 1,200 mm×200 mm. In the walls of the RC specimen, sixteen D10 longitudinal reinforcements were placed, and D10 closed stirrups were placed at a spacing of 280 mm. The same number of D10 longitudinal reinforcements were used in the walls of the half-PC specimens, and three D19 dowel bars protruding from the lower PC wall were grouted into the upper PC wall to enhance the structural integrity. In addition, the half-PC specimens had wall protrusions of trapezoidal shape, having a bottom width of 80 mm and a top width of 70 mm, slightly tapering upward. These protrusions were designed to facilitate the seating of the upper PC wall onto the lower PC wall during assembly process. For the transverse reinforcement in the half-PC specimens, D10 closed stirrups were also placed at a spacing of 280 mm, identical to those in the RC specimen.

The development length of the anchorage reinforcements in the joint region was limited because of the wall detailing, which was 160 mm in the RC specimen and 120 mm (70 mm when accounting for the seating length of the PC slab) in the half-PC specimens. According to Clauses 25.4.3 and 25.4.4 of ACI 318-19, the required development length of the anchorage reinforcement is 150 mm. Therefore, the half-PC specimens did not satisfy this requirement (a more detailed discussion is provided in Section 4). In the slab direction, where the straight part of the anchorage reinforcements was placed, the development length was set to 600 mm in the half-PC specimens to prevent damage and ensure sufficient anchorage performance. This length was determined considering that the required development length of the D10 straight reinforcement, calculated in accordance with ACI 318-19, was 461.9 mm.

2.2 Fabrication of test specimens

Fig. 4 shows the fabrication process for the test specimens. For the half-PC specimens, the upper and lower PC walls, and PC slab were fabricated individually. First, the lower PC wall was positioned, followed by the placement of PC slabs with a seating length of 50 mm on both sides. Subsequently, the top and anchorage reinforcements were placed, and the topping concrete was cast. After curing, the upper PC wall was assembled, and grouting was performed on the sheath tube of the D19 dowel bars to integrate the upper and lower PC walls. Supplementary steel frames were installed to prevent damage during transportation and setup, as shown in Fig. 4(g). The walls and slabs of the RC specimens were cast monolithically.

2.3 Material properties

Five standard cylindrical concrete specimens (ϕ150 mm×300 mm) were fabricated during each instance of concrete casting and grouting, and their compressive strengths were measured on the day of testing in accordance with the ASTM C39/C39M-21 guidelines. In addition, three reinforcement specimens were prepared for each of the two reinforcement types (D10 and D19), and material tests were conducted in accordance with the ASTM A370 guidelines. The material test results summarized in Table 2 represent the average values obtained for the tested specimens. The compressive strengths of the PC slab, PC wall concrete, and grout exceeded the designed compressive strength. However, the compressive strength of the topping concrete in the half-PC specimens and the concrete used in the RC specimen was approximately 85% of the designed compressive strength. The measured yield strengths of the D10 and D19 reinforcements were 455.7 and 516.9 MPa, respectively.

2.4 Test setup

Fig. 5 shows the setup of the quasi-static cyclic loading test. The upper wall of each test specimen was bolted to the supplementary frames connected to the vertical actuator, whereas the lower wall was fixed to the reaction frame. In actual wall systems, the out-of-plane deformation of the wall is minimal within the internal span owing to the constraining effect of the adjacent slabs. Therefore, in this study, the vertical displacement of the test specimen was maintained at zero throughout the experiment using a vertical actuator, as shown in Fig. 5. A horizontal maintenance device was installed to prevent tilting of the supplementary frames connected to the vertical actuator. The test involved the application of repeated lateral loads via a horizontal actuator in the transverse direction. Linear variable differential transformers (LVDTs) were installed to measure the displacement accurately. LVDT 1 was installed

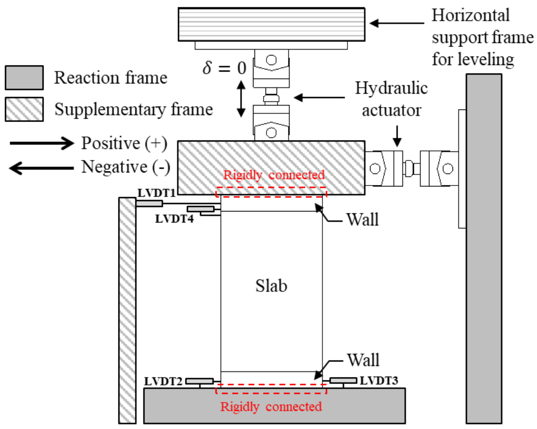

Fig. 5 Test setup (unit: mm)

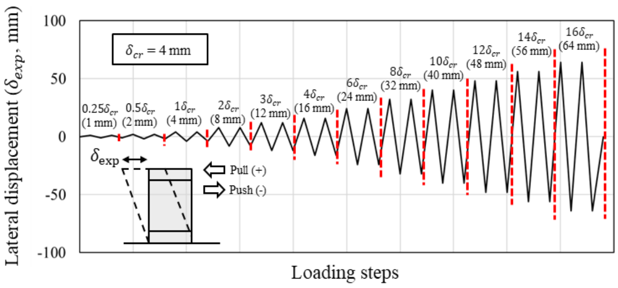

Fig. 6 Loading protocol

to measure the lateral displacement, and LVDTs 2 and 3 were installed to measure the relative slip between the reaction frame and test specimens. In addition, LVDT 4 was installed to measure the relative horizontal slip between the slab and the wall at the slab-wall interface. For the half-PC specimens, the same LVDT was used to measure the relative horizontal slip between the topping concrete and the wall.

Fig. 6 shows the loading protocol for the test specimens. Based on the ACI 374-2 report, the loading protocol was divided into 11 loading steps, and each step was applied twice. However, for some test specimens, loading continued up to the 12th step (lateral displacement; δ_{exp}=±64 mm). The displacement for each loading step was set based on the initial cracking point (δ_{cr}=4 mm) of the pushover specimen, as reported in a previous study (Yun *et al.* 2025). It is noted that the details of the specimen used by Yun *et al.* (2025) are the same as those of the Ho0.5T specimen used in this study.

3. Test results

3.1 Hysteresis response

Fig. 7 presents the lateral load-displacement curves of the test specimens, and Fig. 8 shows the crack patterns in the test specimens at the main loading steps (i.e., the loading step 3; δ_{exp}=±4 mm, maximum lateral loading step, and experiment endpoint). The lateral displacement (δ_{exp}) of the test specimens were calculated by compensating for the slip between the reaction frame and test specimens as follows,

$$\delta_{exp} = \delta_{LVDT1} - \delta_{LVDT2} - \delta_{LVDT3} \quad (1)$$

where δ_{LVDT1}, δ_{LVDT2}, and δ_{LVDT3} represent the measured values of LVDTs 1, 2, and 3, respectively.

In the loading step 1 (δ_{exp}=±1 mm) of the RC specimen, initial cracks occurred at the upper and lower right ends of the specimen, and cracks were observed at the left end before loading step 3 (δ_{exp}=±4 mm). All cracks at the ends were located at the slab-wall interface, and the crack widths increased continuously with increasing lateral displacement. No cracks were observed at any other location except for the slab-wall interface during loading. The maximum lateral load in the positive direction of the RC specimen was 489.3 kN when the lateral displacement was 41.2 mm. In addition, the maximum lateral load in the negative direction was -514.9 kN when the lateral displacement was -37.6 mm. In the loading step 10 (δ_{exp}=±48 mm), concrete spalling occurred at the right ends of the upper and lower parts of the specimen, and serious local damage was observed at the end of the experiment (refer to Fig. 8(b)).

In the case of the Ho0.5T specimen with the 90° standard hook detail, initial cracks were observed at the end of the loading step 1 (δ_{exp}=±1 mm) (refer to Fig. 8(c)). The initial cracks occurred at the slab-wall interface (①), and additional cracks occurred at the interface of the toping concrete-wall interface (②). As the lateral displacement increased, the cracks at the two interfaces continued to expand until the loading step 4 (δ_{exp}=±8 mm). However, from the subsequent loading steps, the cracks at the slab-wall interface (①) propagated more rapidly. Cracks were observed at the topping concrete-PC slab interface (③) in the loading step 8 (δ_{exp}=±32 mm). The maximum lateral load in the positive direction of the Ho0.5T specimen was 397.6 kN when the lateral displacement was 55.2 mm. In addition, the maximum lateral load in the negative direction was -438.9 kN when the lateral displacement was -47.0 mm. After the loading step 11 (δ_{exp}=±56 mm), the surface of the concrete continued to peel off at the end, and simultaneously, the slab-wall interface (①) widened significantly, leading to the failure of the specimen.

The crack patterns and failure modes of the He0.5T specimen with the headed bar detail and the U0.5T specimen with the U-shaped bar detail were almost the same as those of the Ho0.5T specimen (see Figs. 8(d) and 8(e)). The maximum lateral loads of the He0.5T specimen were 378.4 kN and -400.1 kN, respectively, in both directions, when the lateral displacement values were 56.1 mm and -38.1 mm, respectively. In addition, the maximum lateral loads of the U0.5T specimen were 382.6 kN and -456.8 kN in both directions, and the lateral displacement values were 55.6 mm and -52.0 mm, respectively.

For the U0.75T and U1.0T specimens, which had 1.5 and 2.0 times the number of anchorage reinforcements compared to the U0.5T specimen, the initial crack patterns were similar to that of the U0.5T specimen (see Figs. 8(f) and 8(g)). However, in the U1.0T specimen, additional cracks were observed near the interface, extending beyond

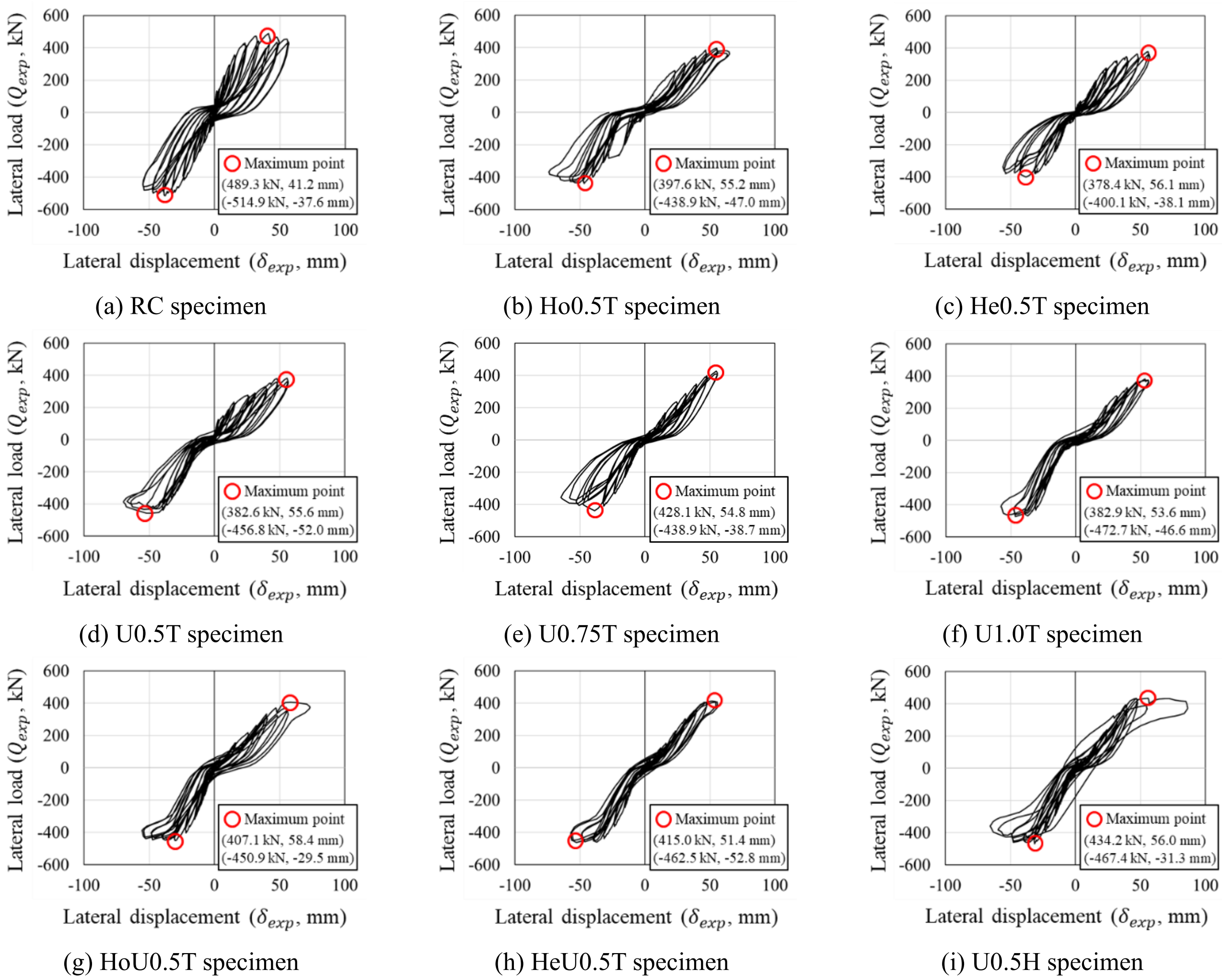

Fig. 7 Lateral load-displacement curves

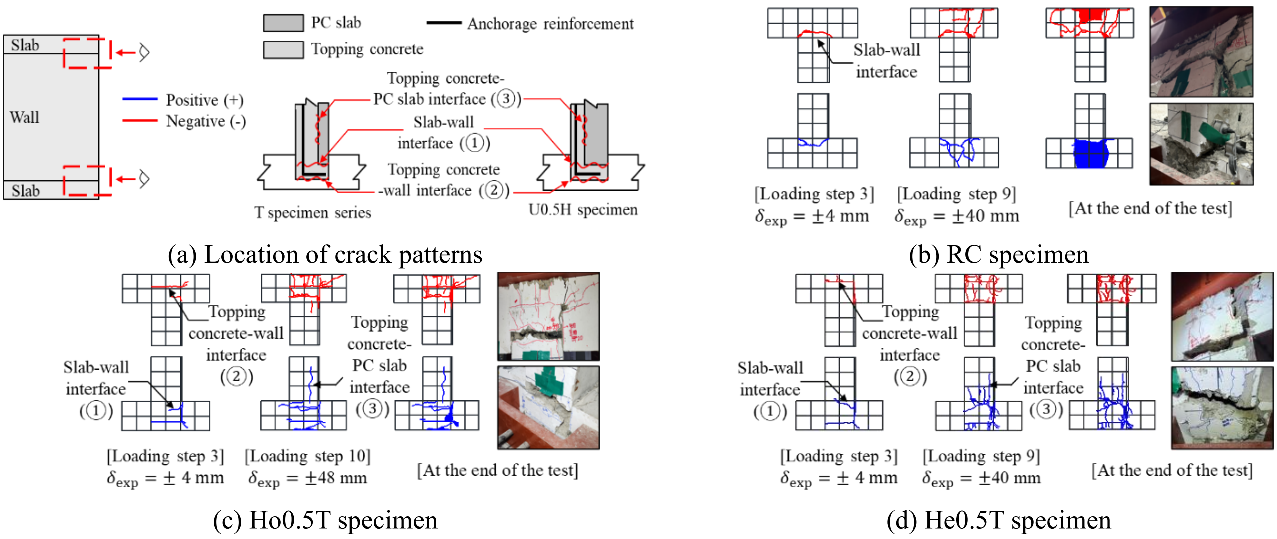

Fig. 8 Crack patterns of test specimens

the initial cracks at the topping concrete-PC slab interface (③) after the loading step 7 (δ_{exp}=±24 mm). In the U1.0T specimen, shear cracks occurred in front of the slab unit at the endpoint of the specimen. The maximum lateral loads of the U0.75T specimen in both directions were 428.1 kN (δ_{exp}=54.8 mm) and -438.9 kN (δ_{exp}=-38.7 mm), and the maximum lateral loads of the U1.0T specimen were 382.9 kN (δ_{exp}=53.6 mm) and -472.7 kN (δ_{exp}=-46.6 mm),

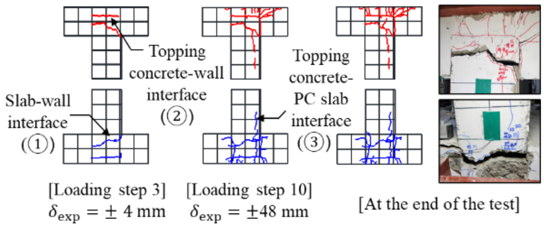

(e) U0.5T specimen

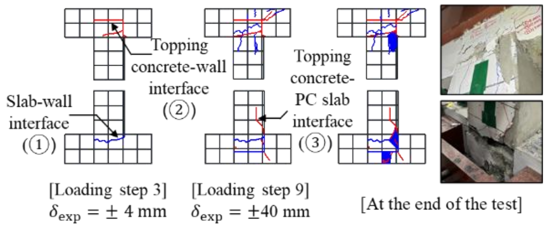

(f) U0.75T specimen

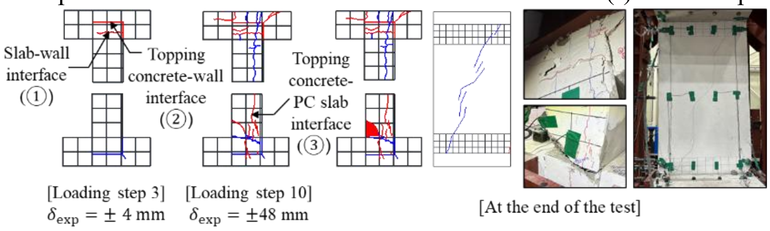

(g) U1.0T specimen

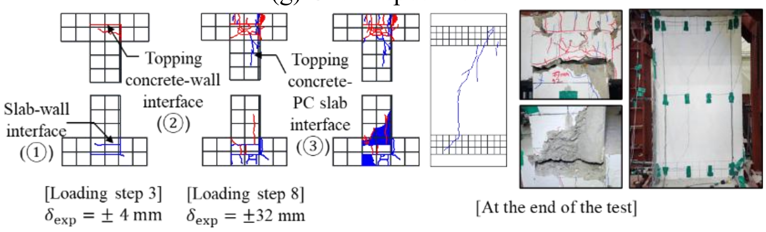

(h) HoU0.5T specimen

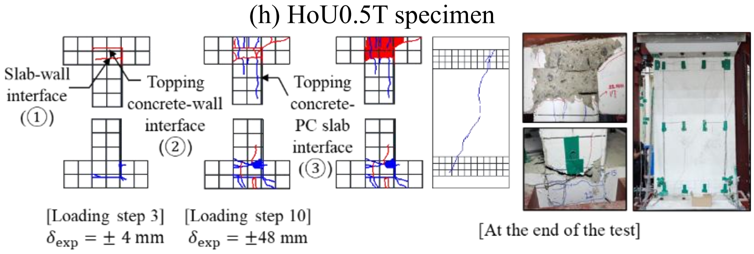

(i) HeU0.5T specimen

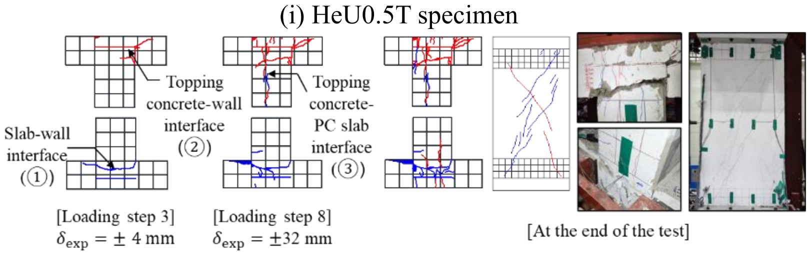

(j) U0.5H specimen

Fig. 8 Continued

respectively.

The initial crack patterns and failure modes of the HoU0.5T (combining the 90° standard hook detail with the U-shaped bar detail) and HeU0.5T specimens (combining the headed bar detail with the U-shaped detail) were similar to those of the U1.0T specimen (see Figs. 8(h) and 8(i)). However, in the HeU0.5T specimen, cracks at the topping concrete-PC slab interface (③) were minimal compared to those observed in the U1.0T and HoU0.5T specimens. The maximum lateral loads recorded for the HoU0.5T specimen were 407.1 kN at 58.4 mm and -450.9 kN at -29.5 mm, in both directions, respectively. For the HeU0.5T specimen, the maximum lateral loads were 415.0 kN at 51.4 mm and -462.5 kN at -52.8 mm.

As shown in Fig. 8(j), the crack pattern and failure mode of the U0.5H specimen with a hollow-core PC slab were similar to those of the U0.5T specimen. In the U0.5H specimen, despite the fact that the topping concrete and PC slab were integrated only through rough surface treatment without the additional reinforcements due to the characteristics of the hollow-core PC slab, the difference in cracks occurring at the topping concrete-PC slab interface (③) was insignificant compared to the U0.5T specimen wherein the topping concrete and PC slab were integrated using truss bars. However, shear cracks were observed at the front of the slab unit even in the U0.5H specimen. The maximum lateral loads in both directions were 434.2 kN δ_{exp}=56.0 mm) and -467.4 kN (δ_{exp}=-31.3 mm).

Table 3 Maximum lateral load of test specimens

Specimen Name	Maximum Lateral Load; Q_{max} [kN] (Ratio of Maximum Lateral Load to that of RC Specimen)	Nominal Strength; Eq. (2) [kN] (Ratio of Maximum Lateral Load to Nominal Strength)	Nominal Strength; Eq. (3) [kN] (Ratio of Maximum Lateral Load to Nominal Strength)
RC	502.1 (1)	449.6 (1.12)	-
Ho0.5T	418.3 (0.83)	319.7 (1.31)	130.0 (3.22)
He0.5T	389.3 (0.78)	319.7 (1.22)	130.0 (3.00)
U0.5T	419.7 (0.84)	319.7 (1.31)	130.0 (3.23)
U0.75T	433.5 (0.86)	384.6 (1.13)	194.9 (2.22)
U1.0T	427.8 (0.85)	449.6 (0.95)	259.9 (1.65)
HoU0.5T	429.0 (0.85)	319.7 (1.34)	130.0 (3.30)
HeU0.5T	438.7 (0.87)	319.7 (1.37)	130.0 (3.38)
U0.5H	450.8 (0.90)	382.9 (1.18)	130.0 (3.47)

The crack patterns at the slab-wall interface (①) and topping concrete-wall interface (②) in the half-PC specimens were mostly similar, while cracks at the topping concrete-PC slab interface (③) exhibited some variations depending on the test specimens. Importantly, across all half-PC specimen series, the point at which the load ceased to increase or began to decrease, was closely associated with the propagation or widening of cracks at the slab-wall interface (①). However, the other cracks (② and ③) did not correspond to any noticeable change in their overall performance. In addition, in the U0.5H specimen with a hollow-core PC slab, multiple diagonal cracks occurred within the slab. This is attributed to the thickness of the topping concrete (=80 mm), which was smaller than those of the other specimen (=140 mm). In other words, as the thickness of the topping concrete located at the slab-wall interface decreases, its contribution to the shear resistance decreases, resulting in an increased shear demand on the hollow-core PC slab, which in turn leads to internal damage within the slab.

3.2 Maximum lateral load

The maximum lateral loads of the test specimens—defined as the average of the absolute values of the maximum lateral loads in the positive and negative directions—were compared with the nominal shear strength of the diaphragm specified in ACI 318-19. Clause 18.12.9 of ACI 318-19 presents the nominal shear strength (V_n) as follows,

$$V_n = A_{cv}\left(\lambda\sqrt{f_c'}/6 + \rho_t f_y\right) \tag{2}$$

where A_{cv} is the sectional area of the diaphragm, λ is the modification factor reflecting the reduced mechanical properties of the lightweight concrete, and ρ_t is the ratio of the area of the distributed slab reinforcements in the diaphragm to the gross concrete area perpendicular to the reinforcements. For the joints between PC members in non-composite and composite topping slab diaphragms, the nominal shear strength is given based solely on the shear friction mechanism of the anchorage reinforcements, as follows,

$$V_n = A_{vf} f_y \mu \tag{3}$$

where A_{vf} is the total area of the shear friction reinforcements within the topping slab and μ is the friction coefficient taken as 1.0λ. According to Clause 18.12.9 of ACI 318-19, the maximum lateral loads of the RC and half-PC specimens should be compared with Eqs. (2) and (3), respectively. However, to evaluate whether the concrete at the slab-wall interface in the half-PC specimens contributed significantly to the shear resistance, the maximum lateral load was also compared with Eq. (2), which considers the combined contributions of the concrete and reinforcement. In this case, A_{cv} was calculated based on the total thickness of the topping concrete and PC slab, and f_c' was determined as the lesser of f_c' for the topping concrete and f_c' for the PC slab.

Table 3 summarizes the maximum lateral loads of the test specimens. The maximum lateral load of the RC specimen was 502.1 kN, which was approximately 17.9% higher than the average maximum lateral load of the half-PC specimens. The nominal shear strength of the RC specimen calculated using Eq. (2) was 449.6 kN, indicating that the maximum lateral load exceeded the nominal shear strength by approximately 11.7%. The maximum lateral load of the He0.5T specimen (which used the headed bar details) was 389.3 kN. Although this value was the lowest among the half-PC specimens, it did not differ significantly from those of the Ho0.5T specimen with the 90° standard hook detail, U0.5T specimen with the U-shaped bar detail, and HoU0.5T and HeU0.5T specimens with combined details. The maximum lateral load of the U0.5H specimen with the hollow-core PC slab was 450.8 kN, which was the highest among the half-PC specimens and was approximately 7.4% higher than the maximum lateral load of the U0.5T specimen. For the U0.75T and U1.0T specimens, which included a relatively large amount of anchorage reinforcement for strength enhancement, almost no improvement in the maximum lateral loads was observed. However, all the half-PC specimens exhibited maximum lateral loads that significantly exceeded the nominal shear strength calculated using Eq. (3) (the average maximum lateral load was approximately 293.2% of the nominal shear strength calculated using Eq. (3)).

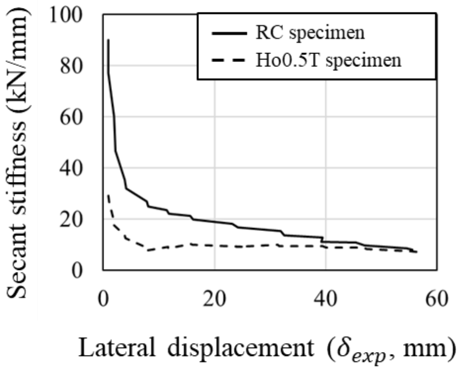

(a) System type

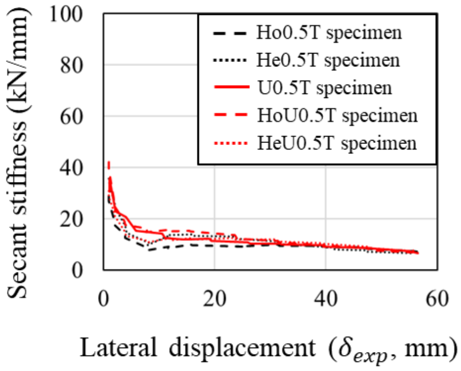

(b) Anchorage type

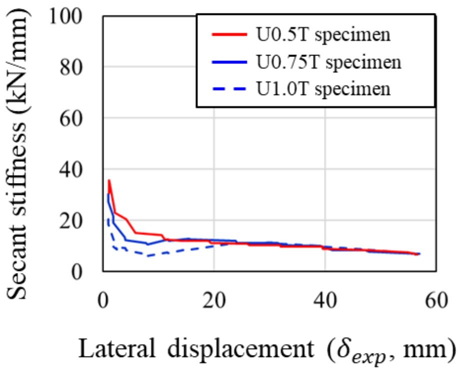

(c) Number of anchorage reinforcements

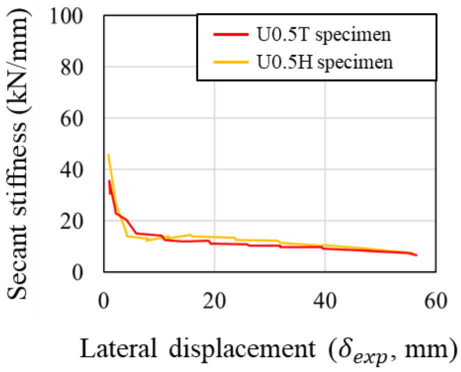

(d) Slab type

Fig. 9 Stiffness retention ability of test specimens

Furthermore, the maximum lateral loads of all the half-PC specimens, except the U1.0T specimen, were higher than the nominal shear strength calculated using Eq. (2). These findings suggest that in the half-PC system, not only the shear friction mechanism by the anchorage reinforcements but also the shear resistance developed at the concrete interface within the joint play crucial roles in resisting in-plane shear forces. However, it should be noted that this contribution of concrete to the in-plane shear resistance was observed in the test specimens where the anchorage reinforcements did not achieve sufficient development length.

3.3 Stiffness retention ability

Fig. 9 presents a comparison of the secant stiffness up to loading step 11 (δ_{exp}=±56 mm) based on the experimental variables to evaluate the stiffness retention ability of the test specimens. The secant stiffness was calculated as the slope of the line connecting the origin to the peak lateral load at each loading step. The graph shows the average secant stiffnesses in both directions. As shown in Fig. 9(a), the RC specimen exhibited a higher secant stiffness than that of the Ho0.5T specimen. Specifically, the secant stiffness of the RC specimen at the 1st cycle of loading step 1 (δ_{exp}=±1 mm) was 90.1 kN/mm, while that of the Ho0.5T specimen was 30.0 kN/mm, approximately one-third that of the RC specimen. This difference is attributed to the fact that the slab and wall were cast monolithically in the RC specimen.

In the half-PC specimens, the secant stiffness at the 1st cycle of loading step 1 (δ_{exp}=±1 mm) varied depending on the anchorage type, ranging from 29.0 kN/mm to 42.0 kN/mm, as shown in Fig. 9(b). The secant stiffness of the HoU0.5T specimen was the highest at 42.0 kN/mm, while that of the HeU0.5T specimen was 30.7 kN/mm, indicating that combining the headed bar and U-shaped bar details did not lead to improved stiffness. No significant difference was observed in the secant stiffness among the Ho0.5T, He0.5T, and U0.5T specimens. As shown in Fig. 9(c), the number of anchorage reinforcements affected the secant stiffness, and the secant stiffness in the initial stage decreased with an increasing number of anchorage reinforcements. The secant stiffness of the U0.5T, U0.75T, and U1.0T specimens at the 1st cycle of loading step 1 (δ_{exp}=±1 mm) were 35.6 kN/mm, 30.8 kN/mm, and 19.0 kN/mm, respectively. The secant stiffness of the U1.0T specimen was approximately half that of the U0.5T specimen. Generally, the initial secant stiffness is largely affected by the sectional resistance of concrete. Therefore, the decrease in the initial secant stiffness observed in the U0.75T and U1.0T specimens is attributed to the reduced effective concrete sectional area within the joint resulting from excessive anchorage reinforcements in the half-PC slab-wall joint. In addition, the U0.5H specimen with the hollow-core PC slab exhibited higher secant stiffness (45.9 kN/mm at the 1st cycle of loading step 1; (δ_{exp}=±1 mm) than the other half-PC specimens, as shown in Fig. 9(d). This is because the thickness of the slab (280 mm) is higher than that of the

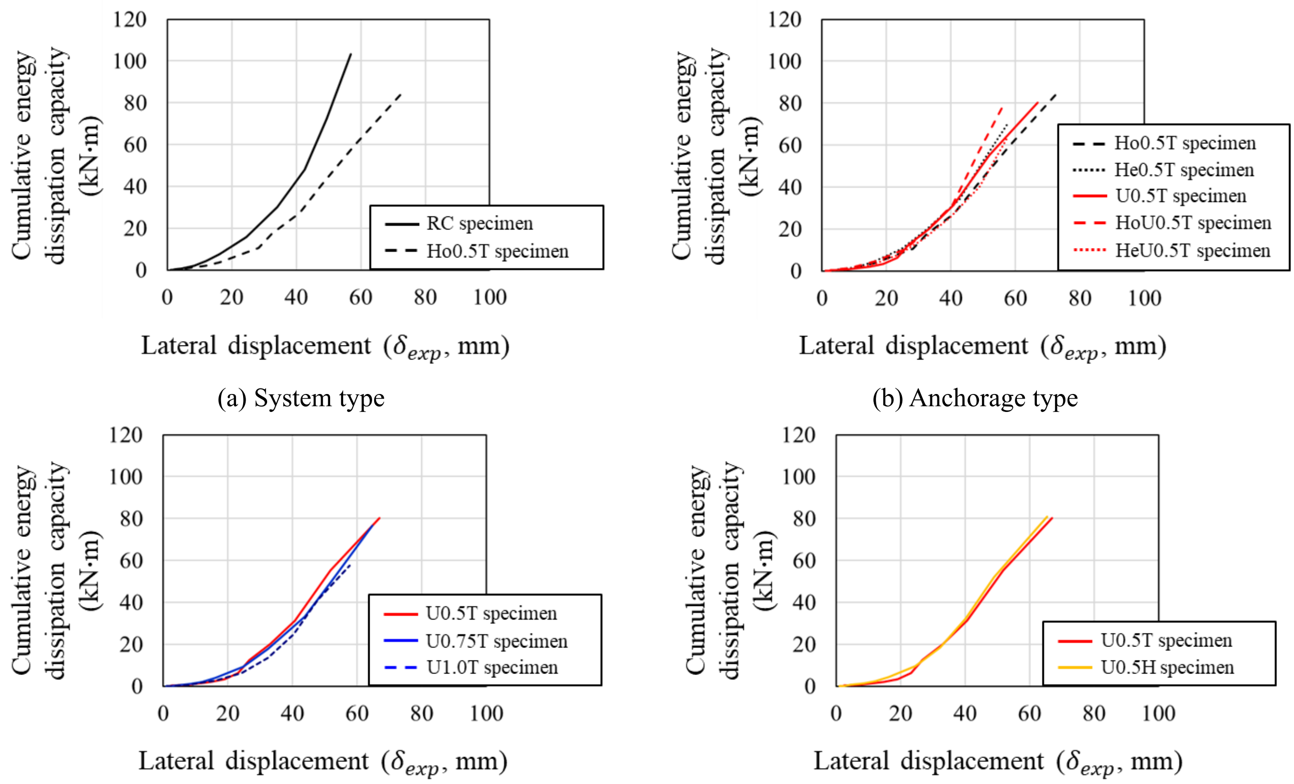

(a) System type

(b) Anchorage type

(c) Number of anchorage reinforcements

(d) Slab type*

*For the U0.5H specimen, the energy dissipation area of the loop was excluded for cases where significantly larger lateral displacement was applied in the positive direction compared to the other specimens.

Fig. 10 Energy dissipation capacity of test specimens

other specimens, which had a thickness of 210 mm.

3.4 Energy dissipation capacity

The energy dissipation capacity is a critical indicator for evaluating the seismic performance of structures subjected to cyclic loading (Choi *et al.* 2018). Fig. 10 presents a comparison of the cumulative energy dissipation capacity based on the experimental variables to evaluate the energy dissipation capacity of the test specimens. The cumulative energy dissipation was calculated as the sum of the internal areas of the lateral force-displacement curves for all cycles, up to the ultimate point in each test specimen. As shown in Fig. 10(a), the RC specimen exhibited superior energy dissipation capacity compared with the Ho0.5T specimen. At the loading step 11 (δ_{exp}=±56 mm), the cumulative energy dissipation capacities of the RC and Ho0.5T specimens were 103.4 kN·m and 59.4 kN·m, respectively. The cumulative energy dissipation capacity of the half-PC specimens according to anchorage type ranged from 55.4 kN·m to 79.9 kN·m at the loading step 11 (δ_{exp}=±56 mm). The cumulative energy dissipation capacity at the loading step 11 (δ_{exp}=±56 mm) of the HoU0.5T specimen was 79.9 kN·m, which was approximately 44% higher than that of the Ho0.5T specimen (=59.4 kN·m). In contrast, the HeU0.5T specimen showed a lower value (62.9 kN·m) than the He0.5T specimen (70.6 kN·m). These results indicate that combining anchorage types does not necessarily enhance the structural performance. In addition, the number of anchorage reinforcements and slab type had minimal effects on the energy dissipation capacity of the test specimens.

The overall structural performances of the test specimens were comprehensively compared and evaluated. The RC specimens exhibited superior load-resisting capacity, stiffness retention ability, and energy dissipation capacity than the half-PC specimens. Nevertheless, the maximum lateral loads of all half-PC specimens exceeded the structural strength requirements specified in ACI 318-19. In the half-PC specimens, the difference in the anchorage type resulted in only minor changes in the structural performance. In particular, despite being a non-standard anchorage type, the U-shaped bar exhibited performance comparable to that of specimens with standard types, such as the 90° standard hook and headed bars. However, in the HoU0.5T specimen, a slight increase in the structural performance was observed in terms of stiffness retention ability and energy dissipation capacity. In contrast, the structural performance of theHeU0.5T specimen tended to decrease. Therefore, future research should include horizontal shear tests that vary the combination of anchorage types to assess the performance changes associated with the anchorage type more effectively. Test specimens with a larger number of anchorage reinforcements (U0.75T and U1.0T specimens) showed no difference in energy dissipation capacity compared with the

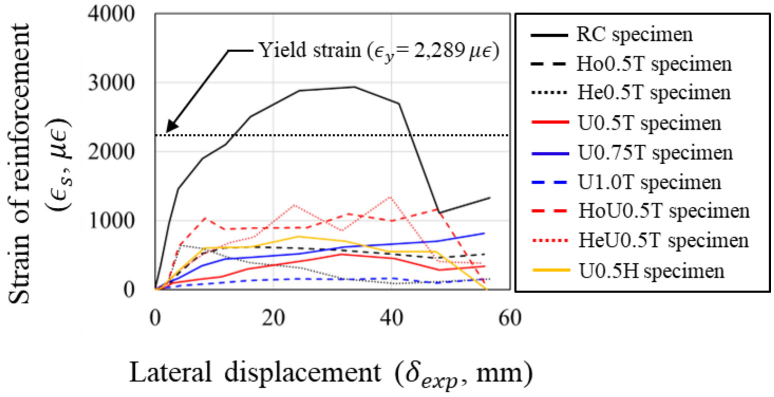

Fig. 11 Lateral displacement-tensile strain of anchorage reinforcement curves

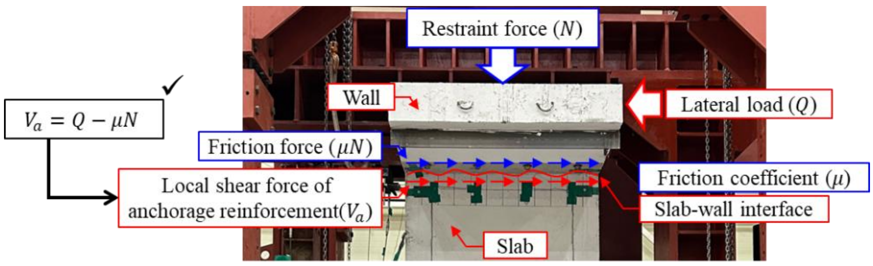

Fig. 12 Method for calculating local shear force of anchorage reinforcement

U0.5T specimen. However, they exhibited lower values than those of the U0.5T specimen in terms of the initial secant stiffness, possibly because the anchorage reinforcements were densely placed within the narrow joint region. Compared with the other half-PC specimens, the U0.5H specimen with a hollow-core PC slab exhibited superior structural performance, except for the energy dissipation capacity. This was attributed to the increase in the total slab thickness from 210 mm to 280 mm, despite a reduction in the topping concrete thickness from 140 mm to 80 mm.

4. Discussions

4.1 Local behavior of anchorage reinforcement

The resistance mechanism of the test specimens against lateral loads comprises three main components: shear friction provided by the anchorage reinforcements, shear resistance of concrete, and friction resistance of the wall owing to restraint forces from the test setup (such as the axial force at the slab-wall interface or within the slab). This study aimed to analyze the local shear behavior of anchorage reinforcements in detail. Fig. 11 shows the relationship between the lateral displacement and tensile strain as measured by the strain gauges attached to the anchorage reinforcement located at the slab-wall interface. In the RC specimen, the anchorage reinforcement experienced a tensile strain exceeding the yield strain (ϵ_y=2,289 $\mu\epsilon$) at failure. In contrast, in the half-PC specimens, the maximum tensile strain in the anchorage reinforcements ranged from 159 $\mu\epsilon$ to 1,347 $\mu\epsilon$, confirming that the anchorage reinforcements did not yield. This outcome was attributed to the insufficient development length of the anchorage reinforcements inside the joint region in the half-PC specimens. The anchorage reinforcement detailing in these specimens did not satisfy the development length requirements specified in ACI 318-19, primarily because of the complex structural detailing of the PC slab-wall joint.

In this study, the local shear force induced by anchorage reinforcements in half-PC specimens was calculated in detail. The local shear force was not calculated using the data measured from strain gauges attached to the anchorage reinforcement, because the strain gauges were attached only to a portion of the anchorage reinforcements. As mentioned earlier and presented in Fig. 12, the lateral load resistance of the test specimens was attributed to three mechanisms (i.e., the shear friction provided by the anchorage reinforcements, shear resistance of the concrete, and friction resistance of the wall induced by the restraint force). Once widening or slip occurred at the slab-wall interface, the shear resistance of the concrete likely decreased rapidly. From this point onward, the test specimens primarily resisted the lateral load via the remaining two mechanisms. Despite the significant widening observed at the slab-wall interface, the lateral load did not exhibit a corresponding drop. This is because, as shown in Fig. 12, even when widening or slip occurred at the slab-wall interface, the vertical displacement was restrained by the test setup, thereby generating a restraint axial force. As a result, the resistance due to interface friction increased significantly. The restraint force measured using the vertical actuator increased with each loading step, reaching an average maximum value of approximately 1,061.1 kN.

Table 4 Lateral load, restraint force, and friction coefficient at the friction coefficient estimation point*

Specimen Name	Lateral Load, Q_{exp} [kN]		Restraint Force, N_{exp} [kN]		Friction Coefficient, μ_{exp} (=Q_{exp}/N_{exp})	
	Positive Direction	Negative Direction	Positive Direction	Negative Direction	Positive Direction	Negative Direction
Ho0.5T	397.6	-425.8	1,014.5	1,009.2	0.392	0.422
He0.5T	378.4	-360.7	975.8	959.9	0.388	0.376
U0.5T	382.6	-432.7	969.5	1,049.2	0.395	0.412
U0.75T	416.1	-391.0	995.5	1,021.1	0.418	0.383
U1.0T	372.3	-418.9	986.5	988.3	0.377	0.424
HoU0.5T	354.8	-404.6	949.5	1,018.3	0.374	0.397
HeU0.5T	393.7	-414.2	996.0	1,019.3	0.395	0.406
U0.5H	434.2	-412.9	1,042.1	1,023.4	0.417	0.403

*At the 1st cycle of loading step 11

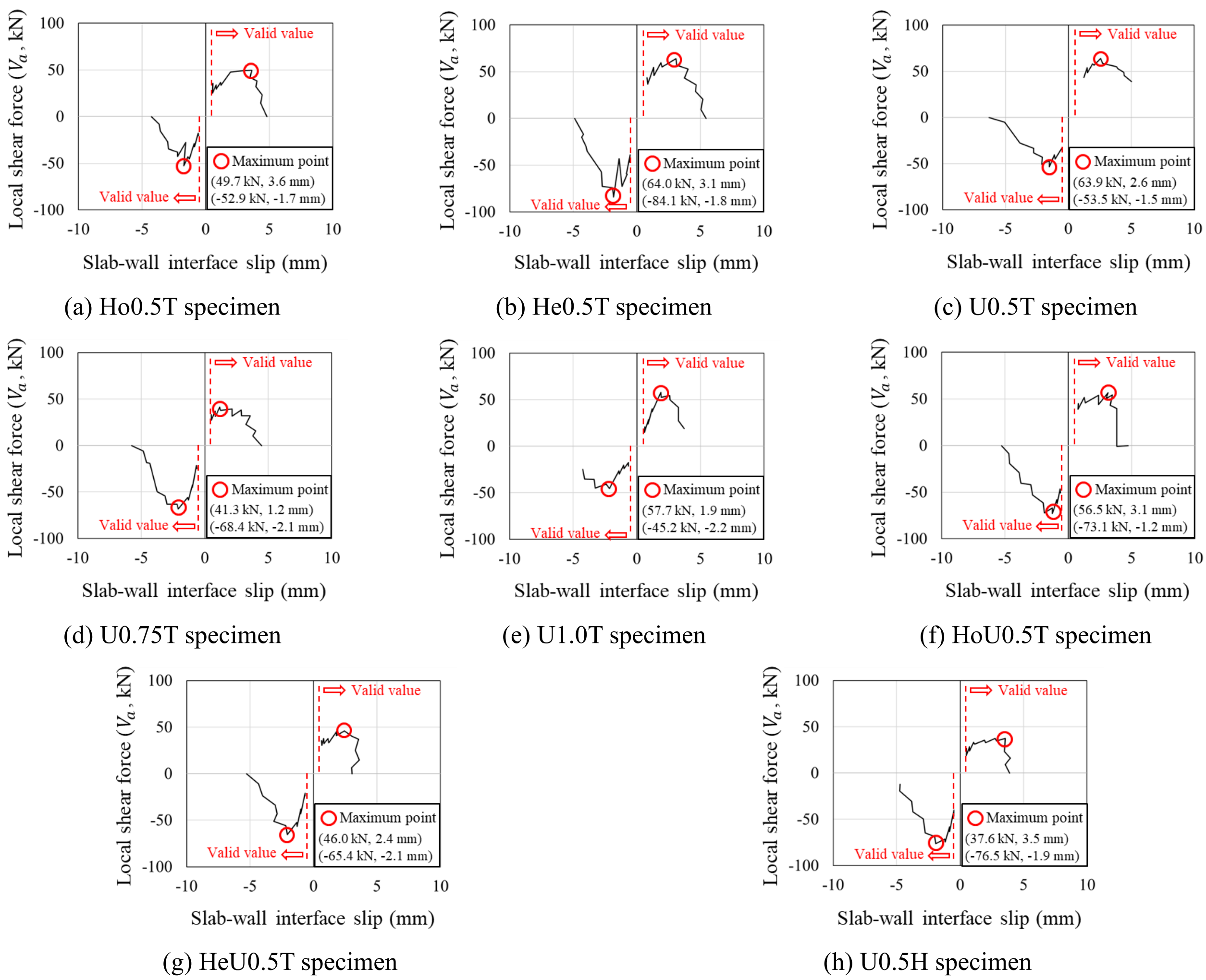

(a) Ho0.5T specimen (b) He0.5T specimen (c) U0.5T specimen
(d) U0.75T specimen (e) U1.0T specimen (f) HoU0.5T specimen
(g) HeU0.5T specimen (h) U0.5H specimen

Fig. 13 Interface slip-local shear force of anchorage reinforcement curves

In this study, the local shear force ($V_{a,exp}$) developed by the anchorage reinforcements was calculated by subtracting the interface friction force ($\mu_{exp}N_{exp}$) caused by the restraint force (N_{exp}) from the lateral load (Q_{exp}) applied to the half-PC specimens, starting from the point where significant widening or slip occurred at the slab-wall interface, as shown in Fig. 12. The point where the shear resistance mechanism of concrete was deemed negligible was defined as the point when the interface slip measured by the LVDT exceeded 0.5 mm, based on previous studies (Loov and Patnaik 1994, Vintzileou *et al.* 2018, Daneshvar *et al.* 2022). The friction coefficient (μ_{exp}) used to determine the interface friction force was calculated by dividing the lateral load by the restraint force in the 1st cycle of loading step 11 (δ_{exp}=±56 mm). This assumed that the interface friction resulting from the restraint force was dominant when the test specimens were subjected to relatively large lateral displacements. As shown in Fig. 11, the tensile strain in the anchorage reinforcements for most half-PC specimens did not increase or even decreased at the loading step 11 (δ_{exp}=±56 mm). This suggests that the contribution of the shear friction provided by the anchorage reinforcements diminished at large lateral displacements.

Table 4 summarizes the lateral loads, restraint forces, and calculated friction coefficients of the half-PC specimens at the loading step 11 (δ_{exp}=±56 mm). The friction coefficients ranged from 0.374 to 0.424, which were lower than the values specified in ACI 318-19 for concrete-concrete interfaces; 1.0 for monolithically cast or intentionally roughened surfaces and 0.6 for as-cast or non-intentionally roughened surfaces. These relatively low values are attributed to the rotation of the test specimens; the gap at the slab-wall interface widened significantly in some areas where the friction coefficient was likely close to zero. Because the friction coefficient in this study was evaluated in an average manner by dividing the total lateral load by the total restraint force across the entire interface, local variations in contact conditions were not distinguished. As a result, even though friction was developed at the regions in contact, the inclusion of the opened regions in the evaluation led to lower apparent values of the friction coefficient.

Fig. 13 shows the relationship between the local shear force of the anchorage reinforcements calculated using the method described in Fig. 12 and the slab-wall interface slip measured by LVDT 4. The lateral load-interface slip curves of the half-PC specimens are presented in Appendix A. The average of the maximum local shear forces in both directions for the test specimens with four anchorage reinforcements were 53.0 kN and -67.6 kN, respectively. The maximum local shear forces in both directions of the U0.75T specimen with six anchorage reinforcements were 41.3 kN and -68.4 kN, respectively, and those of the U1.0T specimen with eight anchorage reinforcements were 57.7 kN and -45.25 kN, respectively. Thus, the local shear force generated by the anchorage reinforcements was found to be lower than the nominal shear strength calculated based on the yield strength of the anchorage reinforcement; (0.5 specimen series=130.0 kN, 0.75 specimen series=194.9 kN, and 1.0 specimen series=259.9 kN; refer to Table 3). In other words, the anchorage reinforcements in the half-PC specimens failed to achieve the expected resistance during the design phase.

As mentioned earlier, the estimation of the local shear force involved two key assumptions. First, the friction coefficient at the slab-wall interface was determined at a large displacement stage, where the contribution of other resistance mechanisms was considered negligible. However, if even a small amount of other resistance mechanisms existed, the calculated friction coefficient would be overestimated compared to the actual value. Accordingly, the local shear force calculated from this coefficient can be interpreted as a lower bound, providing conservative results. Second, it was assumed that the friction coefficient obtained above remained constant from the point of significant interface slip (slip>0.5 mm) until ultimate point. In this case, during the early stage just after significant slip initiation, the actual friction coefficient could be larger than the assumed value, implying that the local shear force may have been estimated somewhat higher than the actual value. Therefore, the early slip region was not analyzed in detail, and the interpretation instead focused on the comparison of the maximum local shear forces. These maximum values can be regarded as conservative estimates.

4.2 Recommendations and future research

In summary, no significant difference was observed in the in-plane structural performance of the half-PC slab-wall joints depending on the type of anchorage. Notably, the 90° standard hook and headed bar details comply with the ACI 318-19 requirements, whereas the U-shaped bar detail represents a non-standard detail. Nevertheless, the U-shaped bar detail exhibited a structural performance comparable to that of standard methods. However, for practical applications, further verification of the out-of-plane structural performance and connection details between the auxiliary (i.e., U-shaped bars) and straight reinforcement is required. The test results for the U0.75T and U1.0T specimens with a relatively large number of anchorage reinforcements showed that excessive anchorage reinforcements within a narrow joint can adversely affect structural performance, resulting in performance degradation. Therefore, to ensure reliable structural performance, avoiding over reinforcement and complex anchorage details is crucial.

In addition, a slight improvement in the structural performance was observed for the HoU0.5T specimen, which combined the 90° standard hook and U-shaped bar details. However, no such improvement was observed for the HeU0.5T specimen, which combined the headed bar detail with the U-shaped bar detail. Therefore, to clearly identify the performance changes depending on the type of anchorage, future studies should include horizontal shear tests with various anchorage combinations as primary variables.

Concrete was found to be an effective contributor to the shear resistance in relation to the in-plane behavior of the half-PC slab-wall joints. Notably, the design method based on Eq. (3) specified in ACI 318-19, which considers only the contribution of anchorage reinforcement, was found to be conservative for evaluating the actual shear strength. This conservative tendency was also observed in Eq. (2), which incorporates the contributions of both the anchorage reinforcement and concrete. However, as discussed previously, the anchorage reinforcements in the half-PC specimens did not fully develop the resistance expected from Eq. (3). This is because the provided development length of the anchorage reinforcements used in this study (=120 mm or 70 mm, considering the seating length of the PC slab) was shorter than the required development length of 150 mm specified by ACI 318-19. To address this discrepancy, Eq. (3) was modified by incorporating the ratio between the provided development length and the required

Table 5 Evaluation of modified nominal strength and maximum local shear force

Specimen Name	Modified Nominal Shear Strength Calculated Using Eq. (4)*, $V_{n,mod}$ [kN]		Maximum Local Shear Force of Anchorage Reinforcements**, $V_{a,max}$ [kN]	Local Shear Force to Nominal Strength Ratio, $V_{a,max}/V_{n,mod}$	
	l_{pro}=120 mm	l_{pro}=70 mm		l_{pro}=120 mm	l_{pro}=70 mm
Ho0.5T	104.0	60.7	51.3	0.845	0.493
He0.5T			74.1	1.221	0.712
U0.5T			58.7	0.968	0.565
U0.75T			64.8	1.068	0.623
U1.0T			55.7	0.919	0.536
HoU0.5T			57.0	0.940	0.548
HeU0.5T	155.9	91.0	54.9	0.352	0.603
U0.5H	207.9	121.3	51.5	0.248	0.425

*For the friction coefficient, the average values of both directions were used.

**The average value of $|V_{a,max}|$ in both directions

development length as follows,

$$V_{n,mod} = \left(l_{pro}/l_{req}\right)A_{vf}f_y\mu \tag{4}$$

where l_{pro} is the provided development length of the anchorage reinforcement and l_{req} is the required development length in accordance with ACI 318-19.

The values obtained using Eq. (4) were compared with the maximum local shear force of the anchorage reinforcements ($V_{a,max}$) derived from the experiment. The results are summarized in Table 5. The ratio of the local shear force to the nominal strength of the half-PC specimens, excluding the U0.75T and U1.0T specimens, was found to have an average of 0.580 when l_{pro} was 120 mm and an average of 0.993 when it was 70 mm. This indicates that the modified nominal shear strength considering the seating length of the PC slab reasonably predicts the actual local shear strength of the anchorage reinforcements in the half-PC slab-wall joints. The main reason for the failure of the anchorage reinforcements to fully develop their intended resistance was identified as an insufficient development length. Therefore, if an alternative anchorage detail that can ensure sufficient development length is introduced into half-PC slab-wall joints with four anchorage reinforcements in this study, both the design intent of Eq. (3) and the in-plane structural performance requirements for diaphragm joints specified in ACI 318-19 can be satisfied regardless of the anchorage or slab type.

The ratio of the local shear force to the nominal strength of the U0.75T specimen was 0.352 when l_{pro} was 120 mm and 0.63 when it was 70 mm, while that of the U1.0T specimen was 0.248 and 0.425 when l_{pro} was 120 mm and 70 mm, respectively. Thus, even when a short development length was considered, the local shear forces of the anchorage reinforcements in the U0.75T and U1.0T specimens remained relatively low. This was attributed to a combination of factors, including a reduction in the effective concrete cross-sectional area within the joint caused by excessive anchorage reinforcements and insufficient development length. Accordingly, the placement of more than six anchorage reinforcements, as detailed in this study, is considered undesirable for achieving adequate anchorage performance. In addition, based on these experimental findings, future research needs to be conducted to develop an analytical model capable of systematically evaluating performance variations with respect to anchorage type and proposing improvement strategies to enhance anchorage performance.

5. Conclusions

In this study, quasi-static cyclic loading tests were conducted on nine full-scale slab-wall joint specimens, with key variables that include the system type, anchorage type, number of anchorage reinforcements, and slab type. The results were used to investigate the lateral load-displacement behavior, maximum lateral load, stiffness retention ability, energy dissipation capacity, and local behavior of anchorage reinforcements. The following conclusions can be drawn from this study:

- The RC specimen exhibited superior load resisting capacity, stiffness retention ability, and energy dissipation capacity compared to all half-PC specimens, primarily because of the monolithic casting of the wall and slab, which ensured structural integrity. In the half-PC specimens, the difference in the anchorage type resulted in only minor changes in the structural performance. In particular, despite being a non-standard anchorage type, the U-shaped bar exhibited performance comparable to that of specimens with standard types, such as the 90° standard hook and headed bars.
- In the half-PC specimen details proposed in this study, a structural performance degradation was observed for more than six anchorage reinforcements. This is attributed to the reduced effective concrete cross-sectional area within the joint caused by excessive anchorage reinforcements. In addition, the U0.5H specimen incorporating the hollow-core PC slab exhibited superior structural performance, except for the energy dissipation capacity, compared with the other half-PC specimens, likely owing to the increased overall slab thickness.
- All the test specimens satisfied the nominal shear

strength requirements for diaphragm joints, as specified in ACI 318-19. Notably, except for the U1.0T specimen, the nominal shear strength of the half-PC specimens exceeded the nominal shear strength calculated by considering the shear friction resistance provided by the anchorage reinforcements and the concrete shear resistance. This suggests that concrete plays a substantial role in the in-plane shear resistance of the half-PC slab-wall joint. However, it should be noted that this contribution of concrete to the in-plane shear resistance was observed in the test specimens where the anchorage reinforcements did not achieve sufficient development length.

• The local shear forces of the anchorage reinforcements in the half-PC specimens were estimated by subtracting the interface friction force caused by the restraining force from the lateral load. The resulting values were lower than the nominal shear strength calculated by assuming yielding of the anchorage reinforcements. In particular, the anchorage reinforcements in the half-PC specimens did not fully achieve their design capacities.

• The modified nominal shear strength, which accounts for the ratio of provided to the required development length specified in ACI 318-19, was proposed and compared with the measured local shear force of the anchorage reinforcements. The modified equation reasonably predicted the local shear force of the anchorage reinforcements for half-PC specimens with four anchorage reinforcements, regardless of the anchorage or slab type. However, in the U0.75T and U1.0T specimens, the local shear force remained below the predicted strength, likely because of the combined effects of the insufficient development length and the reduced effective cross-sectional area of the concrete within the joint. Thus, for the half-PC system with the reinforcement details presented in this study, the use of more than six anchorage reinforcements is not recommended to ensure adequate anchorage performance.

Acknowledgments

This work was supported by the National Research Foundation of Korea (NRF) grant funded by the Korea Government (MSIT) (No. RS-2024-00343740).

References

ACI Committee 318 (2019), Building Code Requirements for Structural Concrete and Commentary (ACI 318-19), American Concrete Institute, Farmington Hills, MI, USA.

ACI Committee 374 (2013), Guide for Testing Reinforced Concrete Structural Elements under Slowly Applied Simulated Seismic Loads (ACI 374.2-13), American Concrete Institute, Farmington Hills, MI, USA.

Arditi, D., Ergin, U. and Gunhan, S. (2000), "Factors affecting the use of precast concrete systems", *J. Arch. Eng.*, **6**(3), 79-86. https://doi.org/10.1061/(ASCE)1076-0431(2000)6:3(79).

ASTM International (2021), Standard Test Method for Compressive Strength of Cylindrical Concrete Specimens (ASTM C39/C39M-21), ASTM International, West Conshohocken, PA, USA.

ASTM International (2021), Standard Test Methods and Definitions for Mechanical Testing of Steel Products (ASTM A370-21), ASTM International, West Conshohocken, PA, USA.

Brunesi, E., Peloso, S., Pinho, R. and Nascimbene, R. (2018), "Cyclic testing of a full-scale two-storey reinforced precast concrete wall-slab-wall structure", *Bull. Earthq. Eng.*, **16**, 5309-5339. https://doi.org/10.1007/s10518-018-0359-z.

Choi, S.H., Hwang, J.H., Lee, D.H., Kim, K.S., Zhang, D. and Kim, J.R. (2018), "Experimental study on RC frame structures strengthened by externally-anchored PC wall panels", *Comput. Concrete*, **22**(4), 383-393. https://doi.org/10.4334/jkci.2015.27.4.451.

Daneshvar, D., Behnood, A. and Robisson, A. (2022), "Interfacial bond in concrete-to-concrete composites: A review", *Constr. Build. Mater.*, **359**, 129195. https://doi.org/10.1016/j.conbuildmat.2022.129195.

Fleischman, R.B., Naito, C.J., Restrepo, J.I., Sause, R. and Ghosh, S.K. (2005), "Seismic design methodology for precast concrete diaphragms part 1: Design framework", *PCI J.*, **50**(5), 68-83. https://doi.org/10.15554/pcij.09012005.68.83.

Fleischman, R.B., Restrepo, J.I., Naito, C.J., Sause, R., Zhang, D. and Schoettler, M.J. (2013), "Integrated analytical and experimental research to develop a new seismic design methodology for precast concrete diaphragms", *J. Struct. Eng.*, **139**(7), 1192-1204. https://doi.org/10.1061/(ASCE)ST.1943-541X.0000734.

Kim, J.H., Choi, S., Lee, Y.J., Jeong, H. and Kim, K.S. (2021), "Experimental study on lateral behavior of precast wide beam-column joints", *Earthq. Struct.*, **21**(6), 653-667. https://doi.org/10.12989/eas.2021.21.6.653.

Kim, S., Kim, H., Kang, S., Hwang, H. and Choi, H. (2023), "Effect of joint details on progressive collapse resistance of precast concrete structures", *J. Build. Eng.*, **69**, 106217. https://doi.org/10.1016/j.jobe.2023.106217.

Kurama, Y.C., Sritharan, S., Fleischman R.B., Restrepo, J.I., Henry, R.S., Cleland, N.M., Ghosh, S.K. and Bonelli, P. (2018), "Seismic-resistant precast concrete structures: State of the art", *J. Struct. Eng.*, **144**(4), 03118001. https://doi.org/10.1061/(ASCE)ST.1943-541X.0001972.

Lee, J.D., Yoon, J.K. and Kang, T.H.K. (2016), "Combined half precast concrete slab and post-tensioned slab topping system for basement parking structures", *J. Struct. Integr. Maint.*, **1**(1), 1-9. https://doi.org/10.1080/24705314.2016.1153281.

Lim, W.Y., Kang, T.H.K. and Hong, S.G. (2016), "Cyclic lateral testing of precast concrete T-walls in fast low-rise construction", *ACI Struct. J.*, **113**(1), 179-189. https://doi.org/10.14359/51688200.

Loov, R.E. and Patnaik. (1994), "Horizontal shear strength of composite concrete beams with a rough interface", *PCI J.*, **39**(1), 48-69. https://doi.org/10.15554/pcij.01011994.48.69.

Pang, R., Xu, Z., Liang, S., Zhu, X. and Hu, K. (2020), "Experimental and analytical investigation on the in-plane mechanical property of discretely connected precast RC floor diaphragm", *J. Build. Eng.*, **32**, 101819. https://doi.org/10.1016/j.jobe.2020.101819.

Ren, R. and Naito, C.J. (2013), "Precast concrete diaphragm connector performance database", *J. Struct. Eng.*, **139**(1), 15-27. https://doi.org/10.1061/(ASCE)ST.1943-541X.0000598.

Tsampras, G., Sause, R., Fleischman, R.B. and Restrepo, J.I. (2017), "Experimental study of deformable connection consisting of friction device and rubber bearings to connect floor system to lateral force resisting system", *Earthq. Eng. Struct. Dyn.*, **47**(4), 1032-1053. https://doi.org/10.1002/eqe.3004.

Vintzileou, E., Palieraki, V., Genesio, G. and Piccinin, R. (2018), "Shear behaviour of interfaces within repaired/strengthened RC elements subjected to cyclic actions", *International Workshop on Advanced Materials and Innovative Systems in Structural Engineering: Seismic Practices*, Istanbul, Türkiye, November.

Yun, C., Kim, J.H., Kim, M., Lee, D. and Kim, K.S. (2025), "Experimental study of joint behavior in half PC wall system subjected to in-plane loads", *J. Korea Inst. Struct. Maint. Inspect.*, **29**(1), 17-26. https://doi.org/10.11112/jksmi.2025.29.1.17.

Zhang, D. and Fleischman, R.B. (2016), "Establishment of performance-based seismic design factors for precast concrete floor diaphragms", *Earthq. Eng. Struct. Dyn.*, **45**(5), 675-698. https://doi.org/10.1002/eqe.2679.

Zhang, D., Fleischman, R.B., Naito, C.J. and Ren, R. (2011), "Experimental evaluation of pretopped precast diaphragm flexure joint under seismic demands", *J. Struct. Eng.*, **137**(10), 1063-1074. https://doi.org/10.1061/(ASCE)ST.1943-541X.0000352.

Zhang, D., Fleischman, R.B., Schoettler, M.J., Restrepo, J.I. and Mielke, M. (2019), "Precast diaphragm response in half-scale shake table test", *J. Struct. Eng.*, **145**(5), 04019024. https://doi.org/10.1061/(ASCE)ST.1943-541X.0002304.

Zhang, H., Li, C., Wang, Z. and Zhang, C. (2020), "Seismic performance assessments of precast energy dissipation shear wall structures under earthquake sequence excitations", *Earthq. Struct.*, **18**(2), 147-162. https://doi.org/10.12989/eas.2020.18.2.147.

Zheng, W. and Oliva, M.G. (2005), "A practical method to estimate elastic deformation of precast pretopped double-tee diaphragms", *PCI J.*, **50**(2), 2-13. https://doi.org/10.15554/pcij.03012005.44.55.

Zhi, Q., Guo, Z., Xiao, Q., Yuan, F. and Song, J. (2017), "Quasi-static test and struct-and-tie modeling of precast concrete shear walls with grouted lap-spliced connections", *Constr. Build. Mater.*, **150**(30), 190-203. https://doi.org/10.1016/j.conbuildmat.2017.05.183.

Zhou, Y., Zhang, B., Hwang, H., Xi, S., Fang, L., Huang, Y. and Yi, W. (2021), "Tensile and shear behavior of box connector for precast concrete shear walls", *Eng. Struct.*, **245**, 112983. https://doi.org/10.1016/j.engstruct.2021.112983.

DL

Appendix A

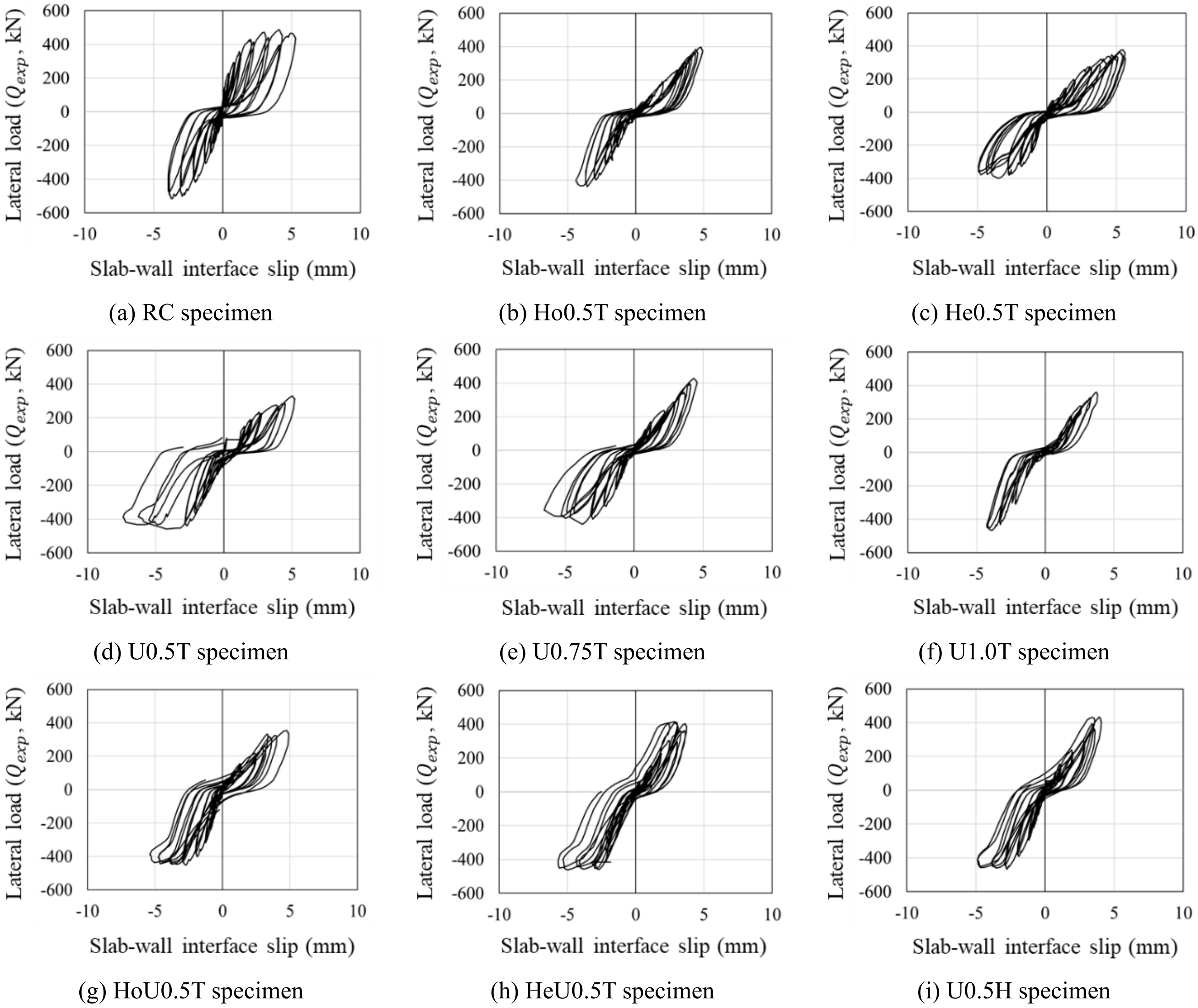

(a) RC specimen (b) Ho0.5T specimen (c) He0.5T specimen

(d) U0.5T specimen (e) U0.75T specimen (f) U1.0T specimen

(g) HoU0.5T specimen (h) HeU0.5T specimen (i) U0.5H specimen

Fig. A1 Interface slip-lateral load curves

Fig. A1 presents the relationship between the slab-wall interface slip and lateral load, as observed in the experiment.